PHOENIX CORPORATION

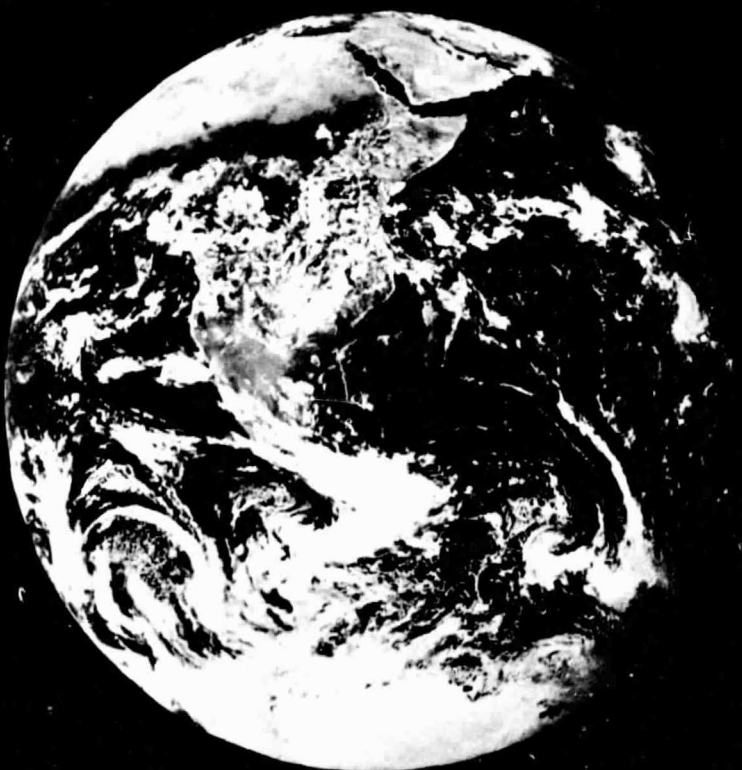

9950 - 582

PHOENIX CORPORATION
1700 OLD MEADOW ROAD, McLEAN, VIRGINIA 22102
(703) 790-1450 • TWX 710-833-0323

SPACE BASED TOPOGRAPHIC MAPPING EXPERIMENT USING SEASAT - SYNTHETIC APERTURE RADAR AND LANDSAT 3 RETURN BEAM VIDICON IMAGERY

Final Report

July 20, 1981

SUBMITTED TO
Dr. Charles Elachi
Jet Propulsion Laboratory
Contract # 955998

by

Dr. Gerald L. Mader
Samuel W. McCandless, Jr.

Phoenix Corporation
1700 Old Meadow Road
McLean, Virginia 22102

TABLE OF CONTENTS

FIGURES

TABLES

ABSTRACT

Topography has long been measured by using stereo photographic image pairs collected from aircraft platforms. Space based stereo observations have not yet been fully exploited but interest in high resolution stereo coverage is increasing and the French SPOT satellite will begin to collect 15 meter stereo pair images of large areas of the earth's surface in 1984.

Conventional stereo coverage has been based on opposite side image combinations using the same sensor type. Same side offset views with identical sensor images have also been used. The Phoenix Corporation, under contract to the Jet Propulsion Laboratory, has been experimenting with quite a different technique for producing topographic information. The approach is based on same side/same time viewing using a dissimilar combination of radar imagery and photographic images. Common geographic areas viewed from similar space reference locations produce scene elevation displacements in opposite direction and proper use of this characteristic can yield the perspective information necessary for determination of base to height ratios. These base to height ratios can in turn be used to produce a topographic map.

The experiment was performed using Synthetic Aperture Radar imagery from the Seasat Satellite and Return Beam Vidicon imagery obtained by the Landsat - 3 satellite. A test area covering the Harrisburg, Pennsylvania region was observed by these two systems in close time proximity and has the added value of having good co-planar ground control points in the common image area.

The techniques developed for the scaling re-orientation and common registration of the two images are presented in this report along with the topographic determination data. The Harrisburg area

is well mapped and its geographic and geologic classification has been studied extensively. Topographic determination based exclusively on the images content is compared to the map information which is used as a performance calibration base.

1.0 STUDY OBJECTIVES AND SCOPE

A major factor influencing target spatial location is the target altitude over the image datum. Figure 1, illustrates the direction and order of magnitude of the ground displacement of target position in the image because of altitude or topographic elevation. This displacement can be large, as indicated, with the direction and magnitude of the displacement a function of sensor type, i.e., Active Sensor = ΔR_s (SEASAT-SAR), Passive Sensor = ΔR_o(Landsat RBV), look angle and the range location of specific topographic areas. In Figure 1, A is the elevation of the image point T, and (a) is the altitude of the satellite, S, with respect to the image datum plane. In a Radar-SAR-Image T will appear at T_s, and would have a ground range displacement of R_s. This displacement is opposite from that of a passive optical-RBV-perspective, in which T would be imaged at T_o.

It is interesting to note that if a target area were imaged optically and with a radar, and properly correlated, all of the information necessary to construct a three dimensional map of the area and to position ground targets at their correct map coordinates could be obtained.

This was the objective of the Phoenix analysis using images of the same geographic area produced by the SEASAT-Synthetic Aperture Radar and the Landsat-3 Return Beam Vidicon Imager.

The implementation of a Topographic Mapping Experiment required the development of a method for detection and correlation of common target points between the two images (geographic pair) to produce the final image products.

The displacements shown in Figure 1 do not include the effects of the earth's curved surface, which may be significant but are well known and were allowed for in study results.

One potential source of error in the ultimate correlation of the image pair is geometric misalignment due to the inclination and resulting platform velocity vector difference between the SAR and RBV images.

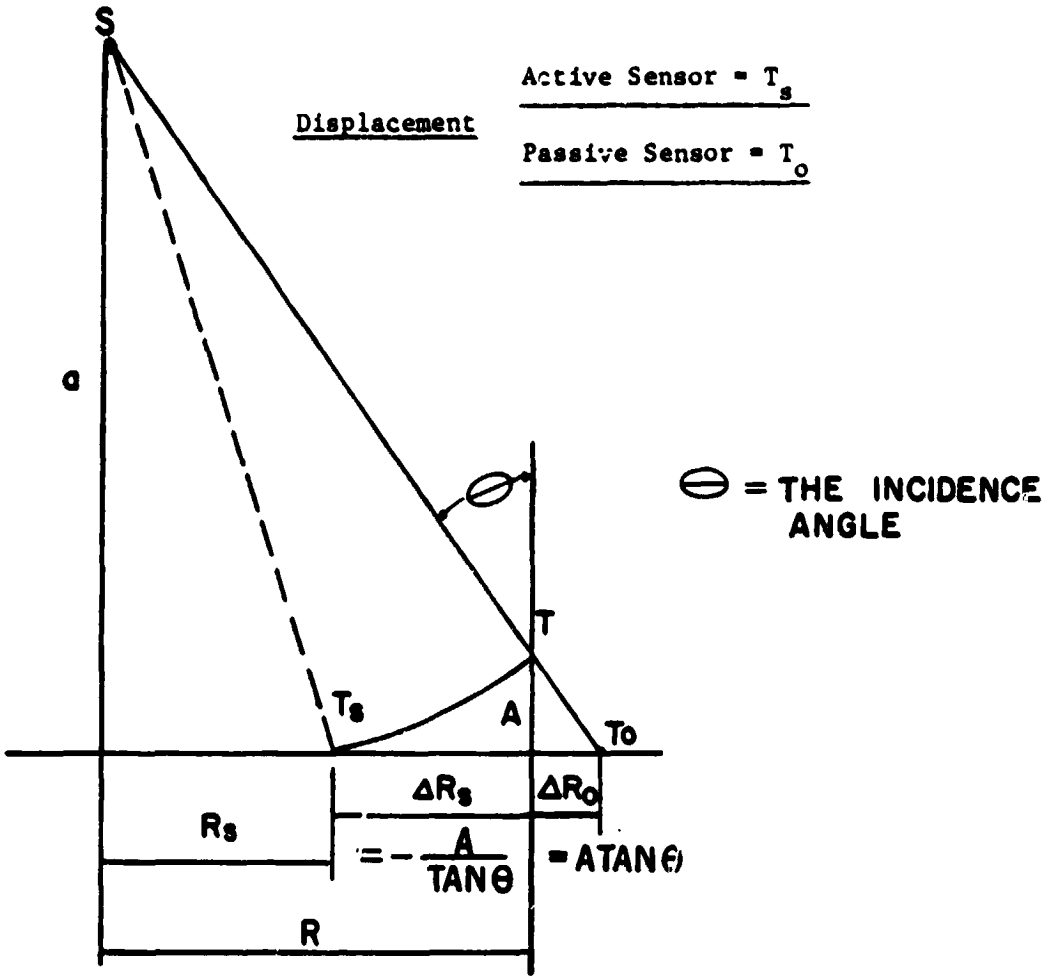

EXAMPLE DISPLACEMENTS $\theta = 23.5^{\circ}$

A	ΔR_s	ΔR_o
1 m	2.3 m	.44 m
5 m	11.5 m	2.18 m
10 m	23.0 m	4.35 m
50 m	115.0 m	21.80 m
100 m	229.9 m	43.50 m
500 m	1150.0 m	218.00 m
1000 m	2299.0 m	435.00 m

Figure 1. Translation of elevated targets to displaced locations in the image plane.

There are also image scale factor variations due to the Instantaneous Field of View differences between the SEASAT SAR and the RBV images.

In the simplest case (i.e., one in which there is no terrain relief and the remotely sensed image returns are not a strong function of illumination aspect, time of day etc.) the effect of rotation and scale factor uncertainty is that all pixels are not shifted the same amount so that the position offset is different throughout the scene.

To the extent that this misalignment is known in advance, it can be determined and was compensated for by digitally resampling (i.e., rectifying) one reference image to align it with the second image. In the studies performed by Phoenix this rectification was accomplished by using mapping equations derived by minimizing residual errors at analyst-selected control points. Bilinear polynominal equations can compensate for differences in scale, aspect ratio, rotation, skew and displacement between images assuming that there are no translations caused by heighting displacement. It is possible to select control points to minimize the heighting effects, (i.e., rivers, highway junctions, airports, ...) and to calculate the control point heighting modulation on the alignment process when it occurs. The residual difference at each control point and the rms value for all control points provide a measure of the registration accuracy.

After registration, alignment, the true offset between the two images is due to heighting translation and residual registration and scaling tolerances. The magnitude of this distortion is a function of:

Θ_i SAR = Incidence Angle of the SAR Image to Particular Ground Points

Θ_i RBV = Incidence Angle of the RBV Image to the Same Ground Points

which are well known quantities.

Using the relationship described in Figure 1 and calculations of Range based on orbit histories, a base to height ratio (relative)

can be calculated and a topographic profile developed. This profile was developed and then compared to the actual map derived heighting translations which were used as performance baseline.

2.0 CONCLUSIONS AND RECOMMENDATIONS

Figure 2 summarizes the degree of success attained by using the image information to determine relief (heighting induced range migration). The idealized or expected shift was calculated by using detailed map information and knowledge of sensor(s) viewing incidence in the map area imaged. The incidence angles were derived from precise knowledge of satellite location and sensor pointing angles contained in attitude/orbit histories. Using this information the range (across the common image area) translation versus heighting relationships were determined. The measured or image(s) derived range of values were attained by first re-sampling the images to a common orientation and pixel scaling base and registering both images to the same ground control point datum; then identifying point targets common to both images and measuring the image to image translation.

Phoenix believes that the correlation between the expected and measured values is within tolerance considerations which include:

Variance - Expected Range of Values

Incidence angle tolerance - minimal effect
Translation (ground range) aspect - minimal effect

Variance - Measured Range of Values

Target recognition tolerance $\pm$ 2 pixels $\simeq$ 70'
Registration tolerance---------- $\simeq$ 85'
Geometric Foreshortening---------- $\simeq$ 100'
in range (SAR Image)

The variance in measured values is created by several uncertainties. One uncertainty is pinpointing the common targets in the RBV and SAR images. It is estimated that these uncertainties could be as much as 2 pixels. However, target enhancements (contrast adjustments) were repeated many times to achieve the best possible edge on perimeter definition and it is felt in many cases that the resulting uncertainty was with 1 pixel and about 35 feet. The 35 feet pixel dimension is based on the re-sampled pixel dimensions. The uncertainty could have been in any of four directions in the planar image.

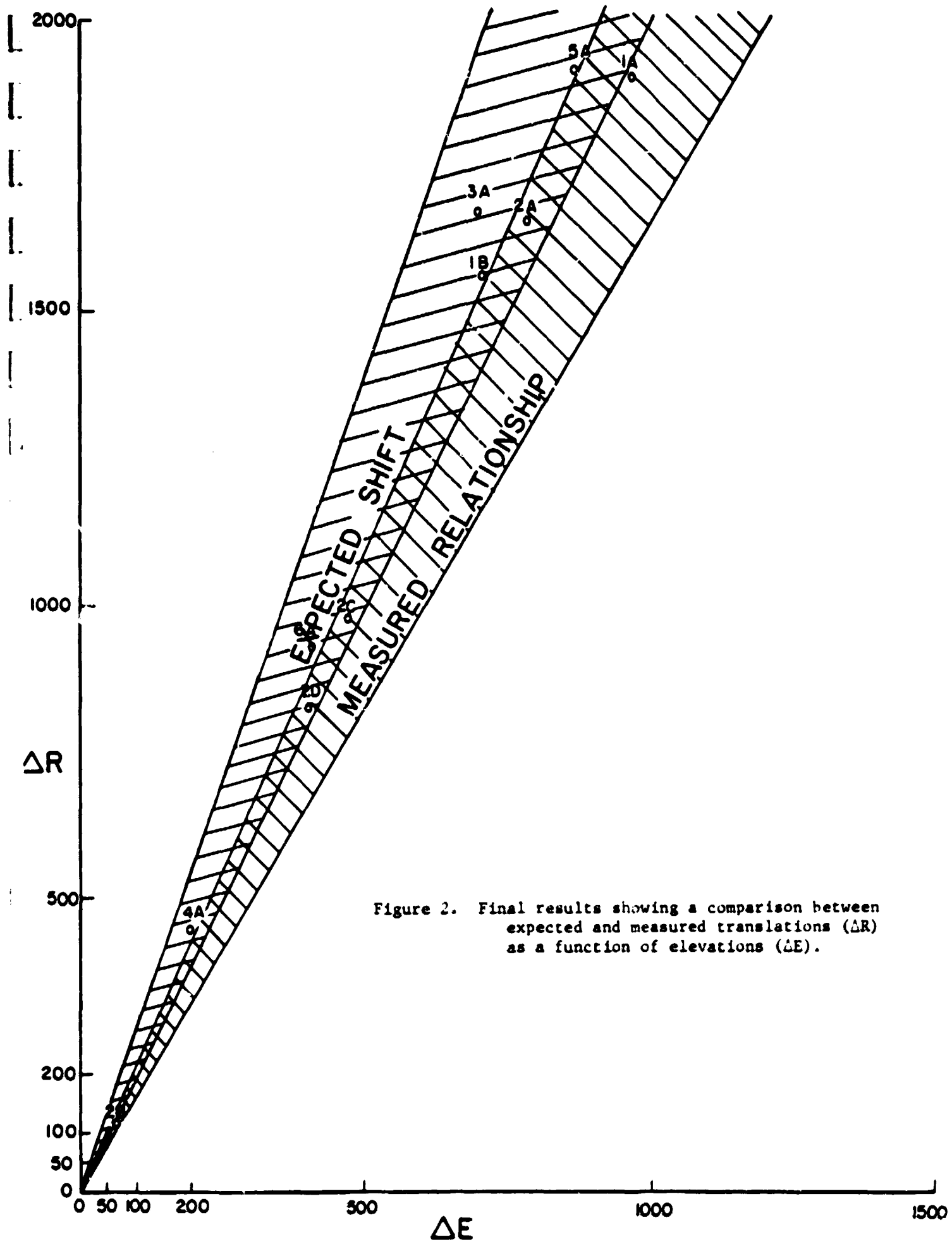

Figure 2. Final results showing a comparison between expected and measured translations (ΔR) as a function of elevations (ΔE).

A second uncertainty are the co-registration tolerances. Registration of each of the images was carefully done using a common set of control points. The results of the interim or mid term report (see Figure 3) revealed that comparison between expected values and measured values produced a fixed offset on bias between the results. Registration was redone using additional control points and making sure that common control points were employed. The initial registration used river area control points, as did the second registration, but due to the radiometric variability or diversity for common targets in the two images, all registration control points were not common to both images. The second registration corrected the systematic offset but some tolerance or error in registration between the two images still exists and is estimated to be about 2½ pixels or 85 feet. As in the case of the target recognition uncertainty the co-registration tolerance could occur in any direction in the planar image field.

It was observed during the experiment that the SAR image was not map or ground range corrected. The Radar Instantaneous Field of View, IFOV, in the range of cross-track dimension is:

$$IFOV = \frac{c}{2\beta \cos\nu}$$

c = The speed of light

β = The bandwidth of the transmitted pulse (FM linear chirp)

ν = The target local grazing angle (radar vector intersection with the local tangent plane)

The quantity $\frac{c}{2\beta}$ is a constant value dependent on radar design parameters and is referred to as the slant range IFOV. To produce a ground range corrected IFOV the $\frac{1}{\cos\nu}$ must be used and the grazing angle ν varies in range across the swath. The SAR image could be made to line up with so-range features on the Harrisburg map but accurate correlation to map scale co-ordinates could not be achieved over the extent of the range dimension. Ground control point registration can partially correct for this condition but large numbers of control points throughout the image would be required to fully correct this anomaly. As a result an offset occurs between measured and expected values and this offset has the effect of decreasing the mea-

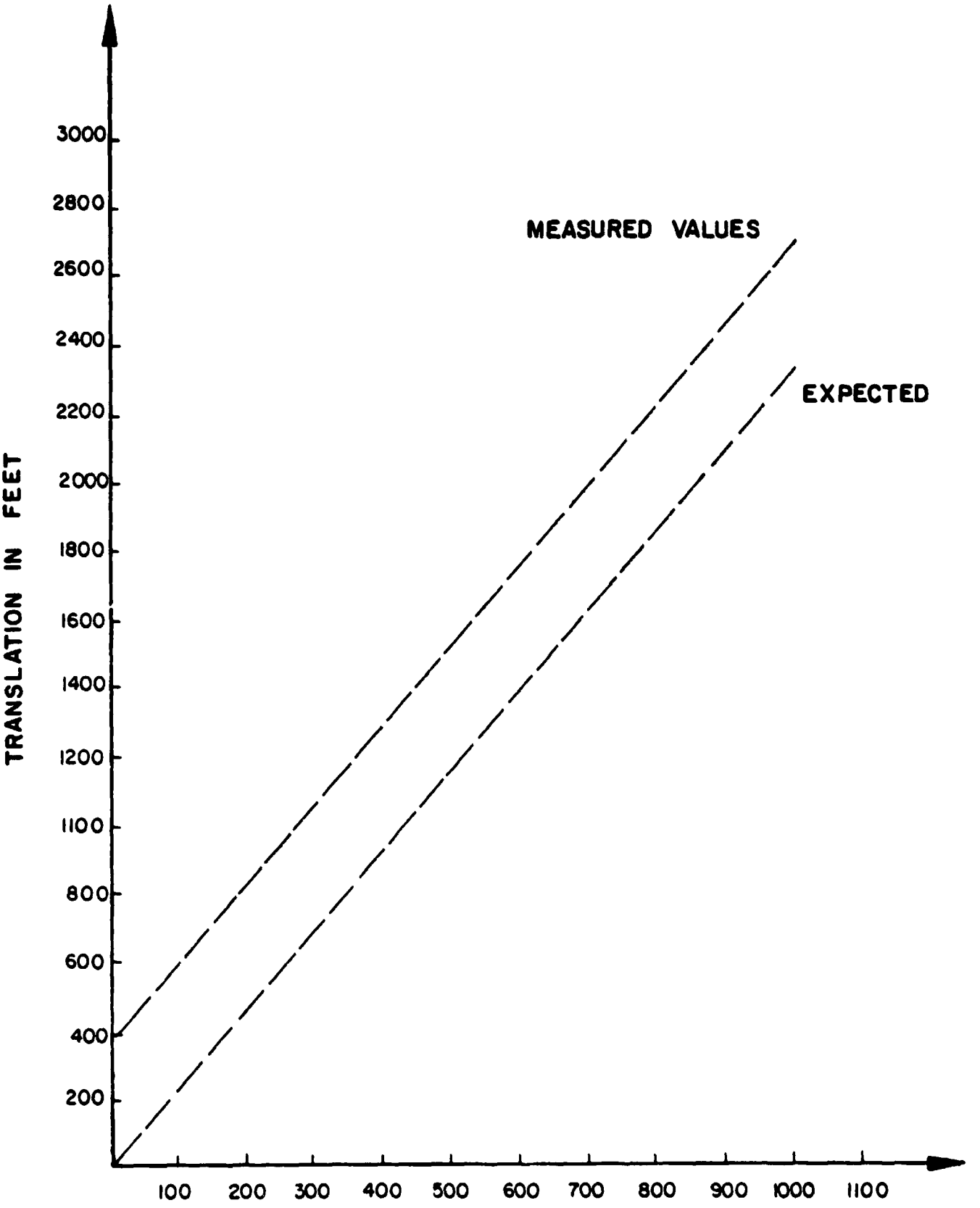

FIGURE 3 - MIDTERM STUDY RESULTS

sured values away from expected values with a clockwise angular shift or in other words the tolerance is directional and not omnidirectional in the planar image field as were prior uncertainties.

Slight variations in the SAR image were also noted in the along track or azimuth direction. This could be due to pulse records being dropped in the Doppler record prior to image signal processing or correlation. This would also produce a foreshortening that would also cause the unidirectional shift noted in the results.

The RBV data matched map co-ordinates very well.

The omnidirectional uncertainties combine to produce:

$$\text{Uncertainty} = \sqrt{70^2 + 85^2}$$
$$= 110'$$

This shift and the directional uncertainty of 110' account for some of the differences noted in Figure 2. Other factors such as the radiometric character of targets in each image, map uncertainties, attitude orbit error buildup may cause larger changes than expected and the degree of difficulty of precise registration make it a prime candidate for further work.

In the authors opinion, the study results support the stereo potential of this unconventional approach and future efforts using this technique should be encouraged. The next opportunity to apply some of the techniques is with SIR-A experiment results using a scheduled Landsat - 3 RBV image confluence.

3.0 STUDY METHODS AND APPROACH

3.1 DATA SELECTION

The important factors influencing data selection were:

1. To select images that were collected closely in time (days) to avoid seasonal or even weather (soil moisture, vegatation differences) related variances.
2. To find an area that possessed a good control point population.
3. To search for a moderate relief scene so that SAR translations not to be so severe as to interfere with the experiment.

These criteria were applied after determining available candidates that merely complied with the more fundamental conditions of SAR and RBV image confluence in a cloud free area (a condition imposed on the RBV not the SAR). The candidates that satisfied these more fundamental conditions were few in number, and the more selective criteria outlined above narrowed the choice to the Harrisburg, Pennsylvania frame(s).

The SAR image, during an ascending orbit, was collected by the SEASAT satellite on the 25th day of September, 1978 at 15:09:11 GMT. The RBV image was collected by the Landsat 3 satellite on the 29th day of September, 1978. Landsat 3 is in a sun synchronous orbit with a 9:30 a.m. equational crossing time. This temporal adjacency complies with the study criteria to select images whose radiometric comparison would not be greatly masked by seasonal variances in target signatures. Study results indicate that this requirement was a necessary one as foliage, clear cut and other seasonal distinctions were very important to RBV and SAR specific point classificaitons.

As shown in Figure 4 the SAR image was collected by an ascending SEASAT orbit with an inclination of 108° and an altitude of 799 kilometers. The Landsat - 3 RBV image was collected by a descending orbit with a 99° inclination and an altitude of 918 kilometers. The subimage used for the study is one scene ≈ 99 km square that was acquired by one of the two RBV cameras. A complete RBV scene is a composite of two each 99 km x 99 km frames taken by two cameras. One camera collects data left of nadir and the other camera is pointing to the right of the nadir trace as the satellite follows its navigation path.

Figure 4 illustrates the relative orientation and positioning of the RBV and SAR images. The image to image interactions that permit contour assessments are based on target/object range translations due to target elevation. As shown in Figure 4 these translations differ in sense or direction and magnitude. The hypothesis used to conduct the study is sketched in the lower portion of Figure 4. The ground range translations in the two images are governed by the viewing perspective. In the RBV image the translation in range ΔR is away from the sensor with magnitude:

$$\Delta R \text{ RBV} = \text{TAN}\theta \times \underline{\text{Object Height}}$$

In the SAR image the translation in range ΔR is toward the sensor with magnitude:

$$\Delta R_{SAR} = \frac{\text{OBJECT HEIGHT}}{\text{TAN}\theta}$$

in both cases θ represents the target local angle of incidence. Just below the plan view of the RBV and SAR image frame overlays, the vector relationships and approximate translations for the study images are illustrated.

3.2 RELEVANT SENSOR PERFORMANCE

Table 1 summarizes some of the important sensor characteristics of the Landsat-3 RBV and SEASAT SAR. The RBV is a panchromatic camera with a ground IFOV of 24m. The RBV sensor produces an image using passive radiometric techniques while the SAR collects a doppler phase history that must be extensively processed with ground based signal processing equipment before an image is created. Although the manner in which these sensors create an image is very dissimilar some important characteristics, that are significant to the type of comparisons made during this experiment, have compatible values. The IFOV's are close together, ground coverage extent for some side viewing is nearly equal and sensor signal to noise ratios are of the same general magnitude.

Figure 4

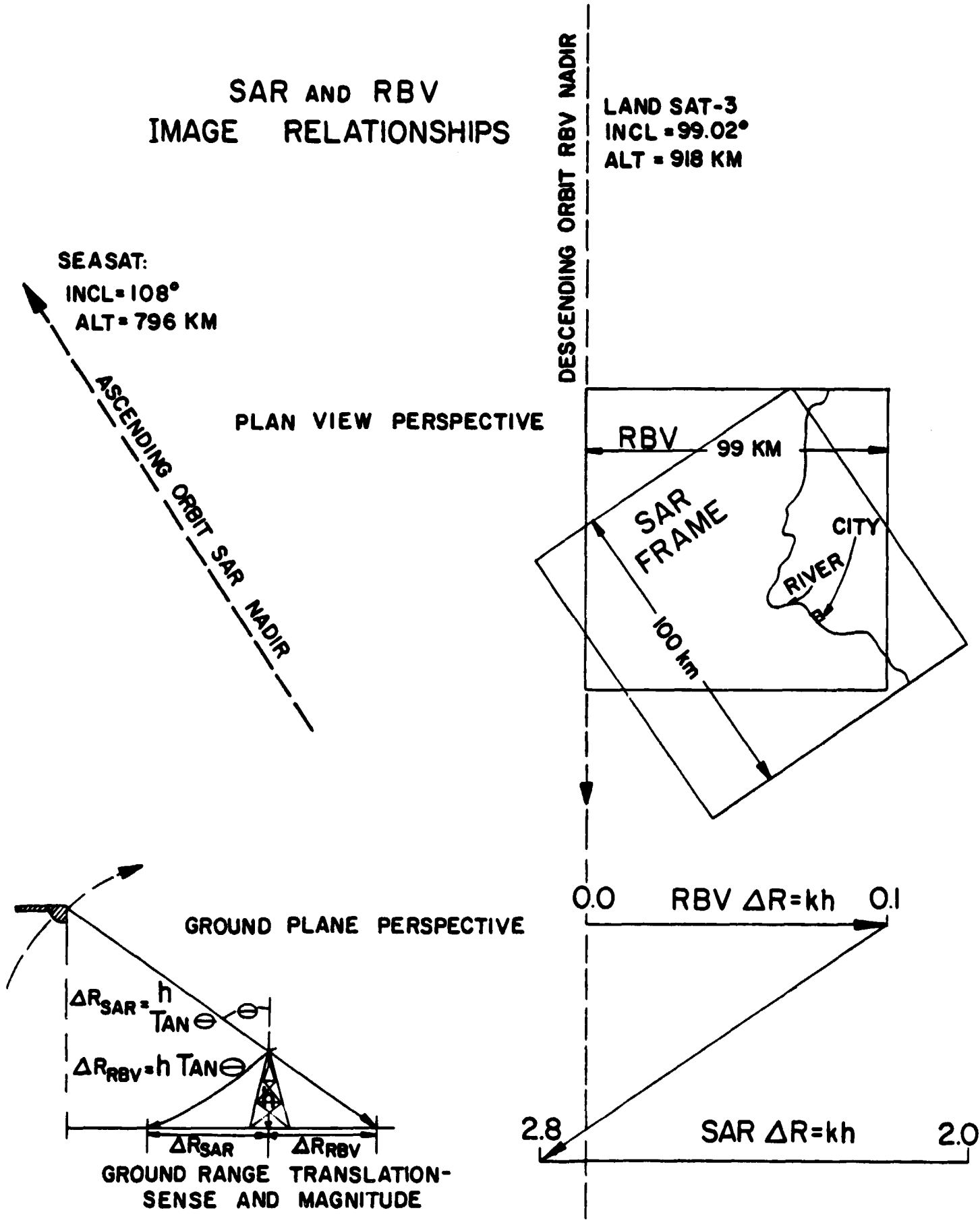
SAR AND RBV
IMAGE RELATIONSHIPS
LAND SAT-3
INCL = 99.02°
ALT = 918 KM
DESCENDING ORBIT RBV NADIR
SEASAT:
INCL = 108°
ALT = 796 KM
ASCENDING ORBIT SAR NADIR
PLAN VIEW PERSPECTIVE
RBV
99 KM
SAR
FRAME
CITY
RIVER
100 km
GROUND PLANE PERSPECTIVE
0.0
RBV ΔR=kh
0.1
ΔR_SAR = h / TAN θ
ΔR_RBV = h TAN θ
ΔR_SAR
ΔR_RBV
GROUND RANGE TRANSLATION-
SENSE AND MAGNITUDE
2.8
SAR ΔR=kh
2.0

TABLE 1

RBV

• RBV Orbit	Sun Synchronous (99° inclination) 918 km
• Spectral Band	Panchronomatic .505 - .750 m
• Signal to Noise Ratio	33 db
• Number of Cameras	2
• Ground Coverage Frame each Camera	99 km x 99 km 2 Frames each Camera=1 Scene Forward Overlap 17 km Side Overlap 17 km
• Ground Resolution IFOV	24 m
• No. of Scan Lines (RBV Photo Sensitive Surface is Read)	4125 Along Track
• Nominal Lens EFL (mm)	236
• Radiometric Correction Error	2 Quantum levels
• Geometric Correction Error	
With GCP's	1 Pixel 90% of the Time
Without GCP's	Attitude/Orbit Errors
Temporal Registration Error	.5 Pixel, 90% of the Time

SAR

• SAR Orbit	Polar (108° inclination) 794 km
• Transmitter Frequency	1275 MHz
• Signal to Noise Ratio	28 db
• Ground Coverage	100 km swath width
• Pulse Repetition Frequency	1463, 1537, 1645 Hz
• Pulse Duration	33.8 sec
• Pulse Bandwidth	19 MHz
• Image Resolution (CCT)	18 m range, 16 m azimuth
• A/D Sampling Rate	45.53 MHz
• A/D Sampling Window Duration	288 sec
• Antenna Dimensions	2 m x 10.5 m
• Antenna Look Angle	20° elevation, 90° azimuth
• Attitude (roll, pitch, yaw) Accuracy	± .5°

By contrast, the radiometric response to theme specific elements in a scene is quite different for each of the sensors. A clear cut area can appear dark (low backscatter/intensity) in the SAR image and may appear bright (high reflected radiance) in the RBV image. Vegetation produces a relatively bright response in the SAR image and is darker in the RBV image. These and many more examples are contained in the exhibit that serves as the major addendum to this report.

Table 2 provides important information about precise orbital and sensor pointing characteristics that must be used to accurately calculate the target local incidence angles in each of the scenes evaluated. Shown in Table 2 are the orbit and sensor pointing characteristics for the SEASAT/SAR at the time that it observed the Harrisburg area. These quantities were used to calculate the range of range translation values expected across the SAR swath width and for specific locations where targets were singled out.

3.3 STUDY METHOD

The study method can be summarized as follows:

1. Several test areas common to both the RBV and SAR images were selected in the Harrisburg scene. Each of the test areas had interesting common features such as radio towers, beacons, power line crossings etc and the added criteria of possessing co-planar control points for common image registration.
2. Each test area was re-sampled to accomplish a co-registration, a common RBV and SAR North realignment and a common pixel or picture unit scaling. After this was completed several contrast enhancement or contrast stretch intensity distributions were made for each of the candidate test areas to highlight the common features selected as point targets.
3. Translation measurements were made and compared with the expected translations using large subimage frames (a few km's) to facilitate accurate measurements.

Maps and image frames for each of the test areas are included in the extensive exhibit that accompanies this report. Table 3 lists the

TABLE 2 SAR ATTITUDE ORBIT INFORMATION

```
DAY HOUR MIN SEC
 258  15   9   7
S/C ALTITUDE USED INSTEAD OF ALTIMETER
S/C ALTITUDE USED INSTEAD OF ALTIMETER
S/C ALTITUDE USED INSTEAD OF ALTIMETER
        1 RECEIVER AGC DC LEVEL    =      0.000  DBM
        2 RECEIVER GAIN            =     69.000  DB
        3 GAIN MODE                       OFF
        4 ECHO SAMPLE GATE SCAN,EN        OFF
        5 ECHO SAMP. GATE PARK,POS=     29.000
        6 ECHO SAMPLE GATE CTR     =    50.611
        7 STC TRIGGER POSITION     =    13.000
        8 STC TRIGGER                     ON
        9 RECEIVER GAIN MODE              MANUAL
       10 RECEIVER GAIN SEL        =     89.000  DB
       11 CAL. SIGN LEVEL          =    -88.000  DBM
       12 XMTR CHRIP RETRIGGER EN        OFF
       13 PRF CODE IN HERTZ        =   1646.750  HERTZ
       14 TRANSMITTED POWER        =    721.063  WATTS
       15 RCVR ECHO AMPL MON  1-4  =     18.621      19.913      17.369      19.913  DBM
       16 RCVR ECHO AMPL MON  5-8  =     18.621      19.247      21.243      22.657  DBM
      *17 NADIR PT. LATITUDE,LONG.=     38. 37. 52.97             280.  0. 55.11  DEG,MIN,SEC
      *18 S/C ALTITUDE,ALTIMETER  =798899.000                743163.631          METERS
      *19 RANGE STDN,EARTH RAD,CUR=  1437.430    6369.869    6374.447             KILOMETERS
      *20 ATTITUDE PITCH,ROLL,YAW =    -0.300       0.187       0.350             DEGREES
       21 POSITION X-,Y-,Z-AXIS  = -4926.992    2689.054    4459.185             KILOMETERS
       22 VELOCITY X-,Y-,Z-DOT   =  5156.611     540.695    5359.389             METERS/SEC.
       23 SLANT RANGE SCALE FACTOR=  175.166     189.741     203.838     217.442  UNITLESS
       24 SWATH VELOCITY         =  6725.841    6725.672    6725.504    6725.337  METERS/SEC
      *25 SLANT RANGES SWATHS 1-2 =   842.261       5.619     851.020       5.677  KILOMETERS,MILISECONDS
      *26 SLANT RANGES SWATHS 3-4 =   860.507       5.741     870.699       5.809  KILOMETERS,MILISECONDS
      *27 INCIDENCE ANGLES        =    19.629      21.436      23.207      24.942  DEGREES
       28 GROUND RANGE COVERAGE   =    24.969      24.977      24.983      24.987  KILOMETERS
       29 TIME DELAYS             =  -211.157    -211.712    -212.279    -212.856  MILISECONDS
       30 RADAR VELOCITIES        =  7184.099    7183.871    7183.643    7183.417  METERS/SEC.
       31 CLOCK ANGLE PERPEN.     =    65.088      65.091      65.094      65.097  DEGREES
       32 DATA LAT.& LONG. SWATH 1=    39. 35. 54.71             282. 39. 38.14  DEGREES,MINUTES,SECONDS
       33 DATA LAT.& LONG. SWATH 2=    39. 41. 28.61             282. 54. 31.75  DEGREES,MINUTES,SECONDS
       34 DATA LAT.& LONG. SWATH 3=    39. 47.  0.43             283. 10. 28.18  DEGREES,MINUTES,SECONDS
       35 DATA LAT.& LONG. SWATH 4=    39. 52. 30.14             283. 26. 27.37  DEGREES,MINUTES,SECONDS
       36 DATA LAT.& LONG. SWATH 5=    39. 57. 57.70             283. 42. 29.28  DEGREES,MINUTES,SECONDS
          RECEIVED POWER-5 KM STEP
       37 SWAT.1- 0, 5,10,15,20,25=    -3.983      -3.829      -3.289      -3.018      -2.975      -3.281  DB
       38 SWAT.2-25,30,35,40,45,50=    -3.281      -3.749      -4.423      -5.381      -6.488      -7.466  DB
       39 SWAT.3-50,55,60,65,70,75=    -7.466      -8.191      -8.569      -8.741      -8.731      -8.758  DB
       40 SWAT.4-75,80,85,90,95,10=    -8.758      -8.734      -8.697      -8.835      -8.899      -9.145  DB

                                                                                ***************
                                                                                REV 1296 MIL
                                                                                ***************
```

Note: Incidence angle is to near range side of 25 km segments of the 100 km swatch.

*Important locations and incidence angle parameters

TABLE 3

MAPS AND AREA/TARGET IMAGES

MAPS

1. Harrisburg, PA area with SAR and RBV image frame overlay.
2. Harrisburg, PA 1/65,500 with area 1 - 6 perimeters.
3. Halifax, PA 1/24,000 with area 1 Peters Mountain outline.
4. Harrisburg East, PA 1/24,000 with area 2 Blue Mountain.
5. Wertzville, PA 1/24,000 with area 3 Cove Mountain and area 6 Lambs Gap.
6. Duncannon, PA 1/24,000 with area 4 Dicks Ridge.
7. Harrisburg West, PA 1/24,000 with area 5 Blue Mountain and Area 2 Blue Mountain.

RBV AND SAR IMAGES

AREA	RBV	SAR
1. Peters Mountain	Full Frame	Full Frame
A - Airway Beacon	Subframe	Subframe
B - Power Transmission Line Crossing	Subframe	Subframe
2. Blue Mountain	Full frame	Full Frame
A - T.V. Tower	Subframe	Subframe
B - Road Crossing	Subframe	Subframe
C - Power Transmission Line Crossing	Subframe	Subframe
D - Power Transmission Line Crossing	Subframe Subframe	Subframe Subframe
3. Cove Mountain - Pine Ridge	Full Frame	Full Frame

Table 3 Con't

AREA	RBV	SAR
4. Dicks Ridge	Full Frame	Full Frame
A - Power Transmission Line Crossing	Subframe	Subframe
5. Blue Mountain	Full Frame	Full Frame
A - T.V. Tower	Subframe	Subframe
6. Lambs Gap	Full Frame	Full Frame
A - Radiotower	Subframe	Subframe

maps and image frames that comprise the exhibit. As indicated, six subimage test area subframes were finally selected after a search of detailed maps and the respective images for recognizable targets. The first map in the exhibit displays the entire Harrisburg area and the SAR-FRAME and RBV-FRAME orientation with respect to the map.

The Phoenix corporation has developed a unique way of displaying images using dot-matrix printer techniques. The image pixel elements are portrayed using an array of dots (or absense of dots) to reproduce grey levels. The images created in this report use 17 grey levels. A special technique to prescribe (program) dot pattern printing and avoid systematic noise or pattern effects has been developed by Phoenix after extensive experimentation. The basic CCT tape assimulation and image production program also includes image rotation on re-orientation (i.e.: North alignment) and pixel scaling (map matching or image to image common scaling) algorithms. Examples of these techniques and image registration are contained in the images that make up the exhibit of study results.

3.4 DESCRIPTION OF TECHNIQUES USED IN EXPERIMENT ANALYSES

The registration, re-orientation and scaling methods and procedures used to facilitate the study are briefly described in this section. Additional details can be supplied to interested readers upon request. The procedures outlined herein were implemented on the Phoenix Corporations Prime 550 computer system.

Figure 4 provides an illustration of how the RBV and SAR images cover the Harrisburg area. The SAR nadir trace is a considerable distance from the image (~ 300 km to the image centerline) while the RBV nadir trace is in the center of the frame. The inclination differences account for the general frame orientation shown.

Using spherical trigonometry the offset angle (discounting attitude differences) can be calculated as follows:

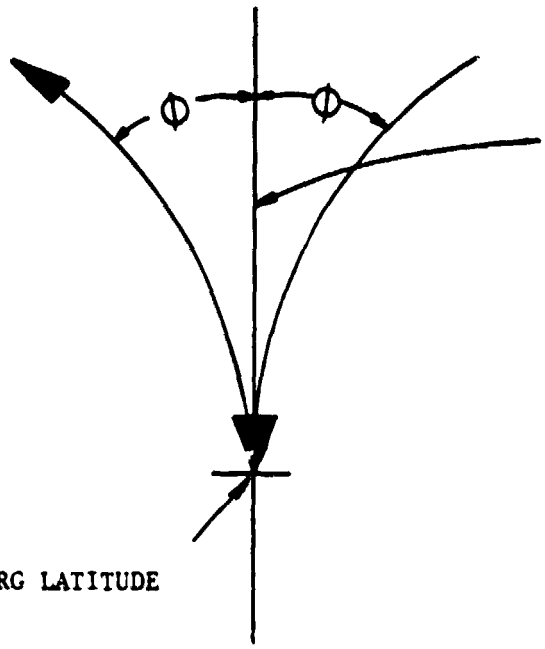

HARRISBURG LATITUDE

LOCAL MERIDIAN

θ ANGLE BETWEEN ASCENDING OR DESCENDING PASSES OF A SATELLITES ORBIT WITH RESPECT TO THE LOCAL MERIDIAN.

$$A_Z = \text{TAN}^{-1}\frac{(\cos i - \frac{N}{R}\cos^2\theta)}{\sqrt{\cos^2\theta - \cos^2 i}}$$

	SEASAT	LANDSAT - 3
N	3	18
R	43	252
i	108°	99.2°

i = Orbital Inclination

θ = Local latitude

N = Number of days before orbit begins a repeat cycle.

R = Number of orbits before a repeat cycle begins.

Harrisburg, Pennsylvania

Latitude = 40° 17'

Figure 5. Orbital crossing angle

SEASAT CALCULATION

$$A_z = \text{TAN}^{-1}\left[\frac{-.309 - .0406}{\sqrt{.58 - .095}}\right]$$

$$A_z = \text{TAN}^{-1}\left[\frac{-.35}{.704}\right] = 26.4^\circ$$

LANDSAT CALCULATION

$$A_z = \text{TAN}^{-1}\left[\frac{-.159 - .04}{\sqrt{.58 - .03}}\right]$$

$$A_z = \text{TAN}^{-1}\left[\frac{-0.199}{.742}\right] = 15.013^\circ$$

In the actual re-orientation programs ground control point locations in each image were used to implement a common image orientation.

Registration

The area around Harrisburg, Pennsylvania, visible in both the SAR and RBV scenes is dominated by the Susquehanna River along with several smaller tributaries and streams. Within the river there are numerous islands and other features clearly distinguishable on the SAR image. Immediately adjacent to the river are several major highways and interchanges visible on the RBV image. These features provided a source of control points on a level surface in an area that is otherwise dominated by variations in relief.

Preliminary inspection of the two images revealed that it would be difficult to find one-to-one correspondences between features or individual pixels between the two images. However, each image showed readily recognizable features that could be identified on topographic maps. A decision was made to register each image separately to a geodetic coordinate system using the clearly seen features in each image and the corresponding map location. Special care was taken to insure that each point selected for control was on the same level surface. Control point locations were shown in the mid term report. Figure 4 indicates that

expected translation to elevation ratios are nominally 0.1 for the RBV scene and 2.0 + 2.8 (far to near range) for the SAR scene dependent on target location. Hence, nominal elevation differences between control point surfaces a few meters apart will result in translation of only several meters; far less than the size of a pixel.

Each of the areas selected for analysis referenced in table 3 were separately registered and resampled using the same control points. The actual registration was done in the following way. Each study area was defined by its latitude and longitude perimeter extent, designated

LATMIN
LATMAX
LONMIN
LONMAX

Within each individual area the latitude and longitude were recomputed with respect to LATMIN AND LONMIN where

$$LAT' = LAT - LATMIN$$
$$LON' = LON - LONMIN$$

For each control point, a LAT and LON value was obtained from the topographic map and a corresponding row and column location I, J was obtained from the respective SAR and RBV images. These matrix and geodetic locations were used in a least squares solution to find the coefficients to the following equations.

$$I = C1 * LAT' + C2 * LON' + C3$$
$$J = C4 * LAT' + C5 * LON' + C6$$

This form allows the image data to be rotated to North, allows for a translation between the new geodetic origin LATMIN, LONMIN and the row, column origin of the image data and also allows different scale changes along the orthogonal axes. It does not allow more sophisticated rubber-sheet capabilities such as skewing or warping of the image. It was felt that most of the gross effects would be removed during the original satellite data processing and in addition each individual area was so small that these effects would not amount to much if they were present. As indicated in the Section (2.0), the SAR range data was not corrected on a pixel by pixel basis for precise slant range to real range geometric

fidelity. This was discovered at the conclusion of the study when comparing measured and expected results. Better registration accuracy would be achieved by resampling SAR CCT's and correcting for this deviation.

The success of our registration algorithm used in this study is estimated from the rms deviation obtained in the following way

$$\sigma_I = \frac{\sqrt{\Sigma(I' - I)^2}}{N}$$

Where I' is the recomputed value of the control points row location and N is the number of control points used. A similar expression was used for σ_J. The values of σ_I and σ_J are summarized for each individual area in Table 4. It is seen that the registration accuracy estimated this way was typically on the order of one or two pixels. Given that we would be looking at elevation differences of about 1,000 feet and corresponding translations of about 2,500 feet or about 70 resampled pixels this registration accuracy was felt to be acceptable. A resampled pixel is 11.12 meters or 36.5 feet. The Table 4 representation is in original RBV SAR IFOV/Pixel units. Comparable 1,000 feet translations are about 30 pixels. In the conclusions section a conservative registration tolerance of 85 feet was assumed.

Resampling

In order to measure displacements due to elevation using the SAR and RBV images, it is necessary that both images be identical in scale and orientation. The previous section explained the basis by which both images are oriented to north. The actual procedure during which this is carried out, while at the same time a scale size is specified to produce a normalized pixel, is called resampling. The resampling is a mapping process by which a grid containing the original data whose row and column orientation and grid spacing is characteristic of the individual sensor is recomputed to some other grid orientation and spacing.

The original data sets were resampled for each of the six test areas. The resampling limits were defined by LATMIN, LATMAX, LONMIN, LONMAX values. The resampling began at the location LATMIN, LONMIN proceeded at

TABLE 4

Summary of Registration Accuracies

Area	SAR		RBV	
	σ_I	σ_J	σ_I	σ_J
1	0.9959	1.7337	1.5112	0.8074
2	0.9958	1.7336	1.5111	0.8077
3	0.9951	1.7340	1.5125	0.8077
4	0.9960	1.7339	1.5116	0.8071
5	0.9959	1.7336	1.5113	0.8078
6	0.9956	1.7338	1.5121	0.8078

constant latitude from LONMIN to LONMAX. The resampling latitude was then increased by Δ LAT and the resampling repeated. The sampling interval in longitude, Δ LON, was defined by

$$\Delta \text{ LON} + \Delta \text{ LAT/COS (LAT)}$$

This ensured that equal areas were sampled in the east-west and north-south directions.

For each LAT, LON position in the resampling grid a corresponding I, J location was found in the image data using the same coefficients solved for in the the registration algorithm. From this I, J value the four image pixels surrounding the LAT, LON position were identified and used to linearly interpolate an amplitude at the LAT, LON position. This procedure is illustrated in Figure 6.

The same latitude and longitude limits were used for each study area for both the SAR and RBV images. The latitude sampling interval was 0.0001 degree for both images. This interval yields a linear sampling distance that is slightly smaller than either the SAR or RBV ground sampling distance. This resampling and registration allowed the translation of features due to elevation changes to be observed and measured by a direct comparison of the two images.

Translation

Changes in elevation are perceived differently by active and passive sensors. This is illustrated in Figures 1 and 4 where a vertical height, h, is viewed by sensor a large distarce away at an angle θ with respect to the local vertical.

Since most elevations will be very much smaller than the distance to the satellite borne sensor and smaller than the radius of the earth, the representation in Figures 1 and 4, showing a locally flat earth, is perfectly satisfactory. However, the assumption of a flat earth cannot be made with regard to the angle θ. Due to earth curvature, this angle can change within a field of view and in general is not equal to the antenna or optics viewing half angles. Figure 7 shows how θ may be computed.

Consider a spherical earth of radius r_e, a reasonable assumption over the distances being considered. Consider also a sensor at alti-

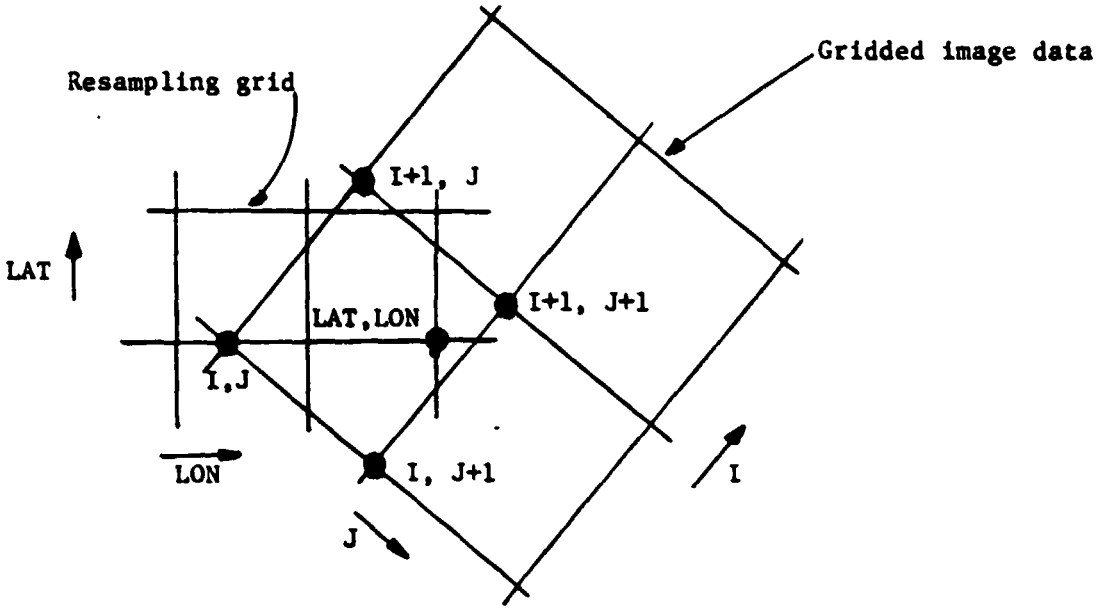

Figure 6. The relation between a point LAT, LON in the resampling grid and the four surrounding points in the image grid used for interpolating a value at LAT, LON.

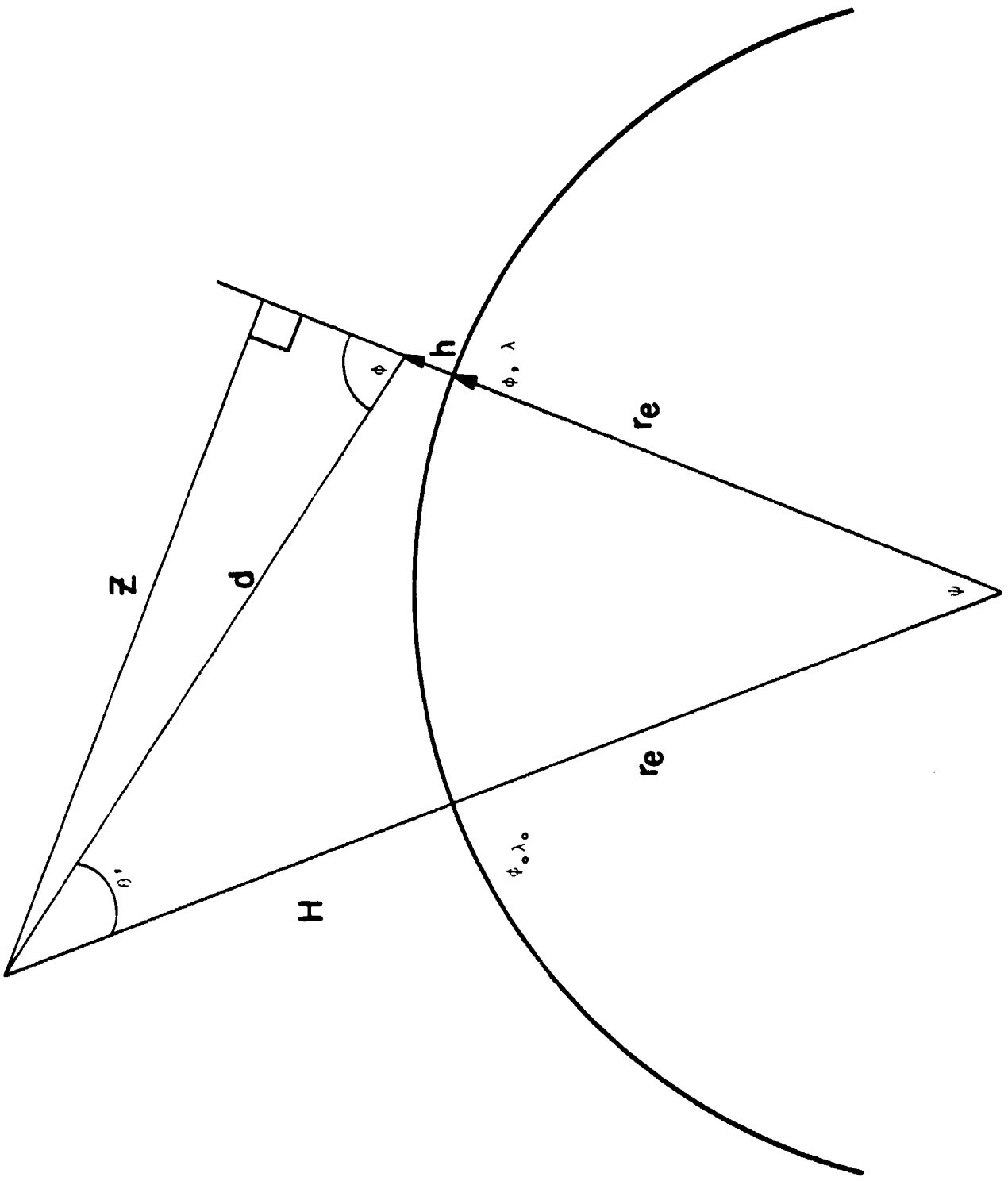

Figure 7. Translation Calculation

tude H whose subsatellite location is at a latitude and longitude given by θ_o, λ_o. This sensor views a height h at location θ, λ, a distance d away. Constructing the line z we see that

$$\theta = \sin^{-1} \left(\frac{z}{d}\right)$$

We also note that

$$z = (r_e + H) \sin \Psi$$

$$d = \left[(r_e + H)^2 + r_e^2 - 2\, r_e(r_e + H) \cos \Psi\right]^{\frac{1}{2}}$$

where $h << r$

and $\Psi = \text{Cos}^{-1} \left[\sin \theta_o \sin \theta + \cos \theta_o \cos \theta \cos (\lambda - \lambda_o)\right]$

For a given sensor location, we are now able to compute the expected translations due to elevation as a function of object location.

To note the magnitude of this effect consider an active sensor with an angle, θ', of 20^o (depression angle = 70^o). The flat earth approximation would set $\theta = 20^o$ and compute a translation for a 100 m elevation of 274.7 m. Such a sensor at an altitude of 800 km would be viewing objects displaced an angular distance $\Psi = 2.5^o$. Using $r_e = 6371$ km we find for this case $\theta = 21.5^o$. This gives a translation of 253.9 m for the same 100 m elevation. Hence, for a system like SEASAT, a flat earth approximation would yield translations in error by about 8%.

Inclination angles were calculated using target local geometrics and the relationships described above. These relationships are shown in Figure 8.

3.5 MEASURED RESULTS

Table 5 lists the measured results obtained from each of the SAR and RBV target subframes contained in the exhibit. The x and y distances to each target were accurately measured from the lower left corner of each subframe which serves as a common registration datum point. The location of the target in the SAR frame was determined and the target/local inclination angle calculated which specifies the translation value (2.0 to 2.8) and this was used to produce a ΔR ΔE relationship in Figure 2. Figure 2 is reproduced as part of this section. In-

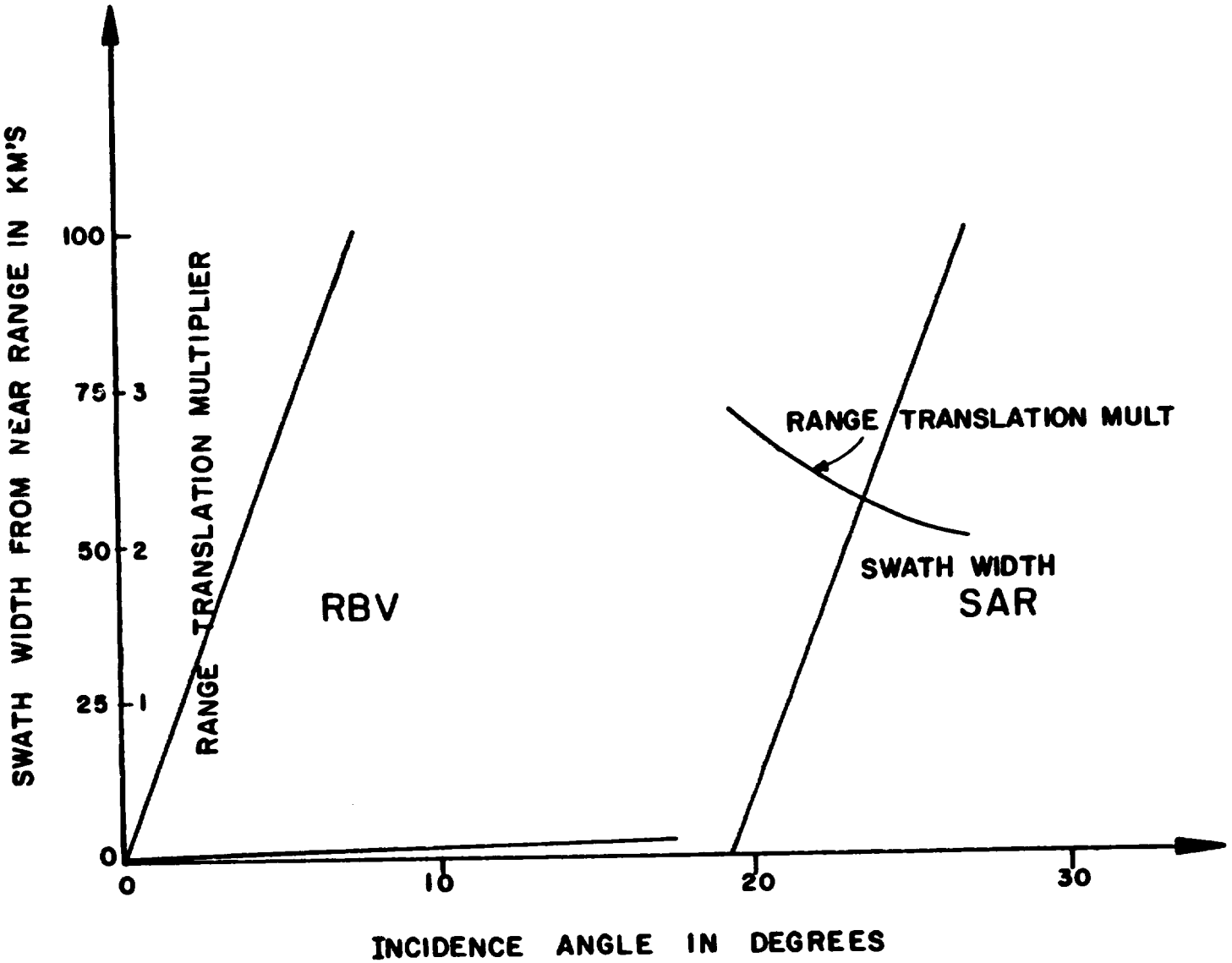

Figure 8. SAR RBV $\Delta E/\Delta R$ Relationships

TABLE 5

Measured Translations

Area	Target	Δx (inches)	Δy (inches)	ΔR (feet)	Translation/Height Ratio	ΔE (feet)
1	A	2-12/16	1-4/16	1918	2.2	872
1	B	2-1/16	1-7/16	1556	2.2	707
2	A	2-6/16	1-2/16	1666	2.1	793
2	B	2/16	2/16	115		55
2	C	1-4/16	1	980		467
2	D	1-8/16	15/16	839		399
3	A	2-6/16	1-13/16	1678	2.4	699
4	A	11/16	2/16	453		189
5	A	2-11/16	1-6/16	1906	2.2	866
6	A	9/16	1-8/16	933	2.3	406

Scale 652' per inch longitude

545' per inch latitude

dividual target locations are shown in the reproduced version of the figure. Accounting for the tolerance variations and SAR range distortions described in Section 2.0 the comparison is technique validating.

A similar experiment should be conducted using the upcoming SIR-A information. One or more of the principle investigation areas planned for SIR-A should be designated for the repeat analysis.